Wiley Online Library
Early View publication on www.wileyonlinelibrary.com
(issue and page numbers not yet assigned;
citable using Digital Object Identifier – **DOI**)

Ann. Phys. (Berlin), 1–9 (2016) / DOI 10.1002/andp.201500317

annalen der physik

Original Paper

Accelerating spontaneous emission in open resonators

Pavel Ginzburg[1,2,*]

Received 15 October 2015, revised 18 October 2015, accepted 14 March 2016
Published online 15 April 2016

Strength of light-matter interactions and radiative dynamics of emitters could be controlled with structuring of electromagnetic environment. While local and cross density of electromagnetic states are routinely used for predicting total and radiative decay rates in the weak coupling regime, resonant nanostructures offer going beyond this description, giving rise to new phenomena. Correlated time-evolution of a strongly coupled emitter-nanoresonator system and nonradiative channels are shown here to predefine the radiative decay dynamics and lead to substantial shortening in characteristic emission times. Quantum formalism, based on stochastic Hamiltonian treatment of radiative and nonradiative processes, was generalized for describing light-matter interactions in vicinity of open nanoresonators. The developed theory was subsequently applied to spontaneous emission dynamics of emitters, situated next to metal surfaces, supporting stopped light resonant conditions. Over four orders of magnitude lifetime shortening was predicted to be detectable in the far-field. The interplay between strong and weak coupling regimes, enabled by resonant nanostructures, could serve as a platform for ultrafast opto-electronic components, fluorescent labels and others.

1 Introduction

Many fundamental phenomena and practical applications are enabled by control over light-matter interactions with designing electromagnetic modes of the vacuum. Purcell effect, describing acceleration or suppression of spontaneous emission rate of an emitter in a cavity [1], is one of the most famous examples on electromagnetic modes design. Foundations of cavity quantum electrodynamics provided tools for rigorous description of light-matter interaction dynamics with both light and matter quantized [2]. For a single mode, the interaction strength, tailored by structuring, depends on two key parameters. The first is a quality factor (Q) of a cavity mode, while the second one is it's modal volume (V) [3, 4]. The influence of both Q and V could be captured simultaneously by introducing the local density of states (LDOS) concept via electromagnetic Green functions approach [5]. However, in the later case, the direct intuitive relation to the spatial structure of individual modes might be less transparent, since the impulse response is spanned by an infinite number of eigen functions [6]. Performances of high-Q photonic cavities are based on retardation effects (photon recycling strengthen the interaction), and, as the result, their modal volumes are limited from below by classical diffraction limit [7]. On the other hand, noble metal (plasmonic) structures, having negative permittivities at visible and infra-red spectral ranges could support highly localized modes, not limited by this effect [8, 9]. Majority of plasmonic cavities have quality factors below hundred due to inherently high material losses [10], with few exceptions available, e.g. [11]. This near-field type of local intensity control, provided by nanostructures, enables enhancement of radiative decay rates via nano-antennae concept [12, 13], and facilitates approaching strong coupling regime of interaction [3, 14–19]. Theoretical frameworks for analysis of light-matter interactions, tailored by plasmonic structuring, are under extensive studies nowadays, e.g. [20, 21], including full quantum treatment of hybrid systems [22]. Nanoscale resonators could be also employed for controlling stimulated emission, where the near-filed feedback replaces traveling phase in a cavity. This concept, coined by the name spaser [23], was attempted for experimental demonstration in various systems. The main deference between spaser and plasmonic nanolaser is the degree of confinement – while the first one operates in completely quasistatic regime [24, 25] (if random-lasing effects can be ruled out), the later has at least one dimension where retardation effects take

* Corresponding author E-mail: pginzburg@post.tau.ac.il
[1] School of Electrical Engineering, Tel Aviv University, Tel Aviv, 69978, Israel
[2] ITMO University, St. Petersburg, 197101, Russia

place [26–29] (for additional discussion see [30]). Spasers were also proposed for biomedical applications [31]. Additional advantage of nanoscale resonators is their potential ability to support ultra-fast interaction regimes [32, 33], associated with fast relaxation of electrons in a metal, carriers' injection mechanisms and others. However, majority of experimental demonstrations and theoretical predictions of this kind are described with either semi-classical tools (without quantizing electromagnetic fields) or by applying the Fermi Golden Rule, assuming the weak coupling regime of interaction. Furthermore, nano-resonators, being inherently open in majority of cases, enable pathways for direct spontaneous emission to the far-field, without being coupled to localized modes. Those direct radiative channels have several advantages over conventional cavities, as will be discussed hereafter. It is worth noting, however, that open nature of nano-resonators is rather related to technological aspects and, in principle, is not fundamental.

Here, rigorous quantum analysis of coupling and dissipation mechanisms in open nano-scale resonators is developed. Stochastic Hamiltonian approach was applied for description of competitive decay channels – direct spontaneous emission to the free space and nonradiative quenching, resulting from electromagnetic coupling to dark (weakly radiating) modes of a structure (nano-resonator). Phonon scattering and/or other effects, causing the depopulation of excited state could be straightforwardly included too. The developed unified formalism enables governing the full quantum dynamics of the interaction, including the strong coupling regime. Furthermore, it was shown, that three fundamental numbers, deductible from general approximations, basic experimental data, and classical electromagnetic modeling, characterize open nano-resonator systems. This formalism was used to explore spontaneous emission dynamics in the vicinity of a metal surface (Fig. 1). It was shown, that the fundamental limit of a radiative decay rate enhancement by an arbitrary flat surface with translational symmetry can be surpassed by introducing both quenching and strong coupling mechanisms. While the first one accelerates the total decay rate and reduces the overall quantum yield, the strong coupling offers dynamical control and re-radiation of spontaneous emission directly to the far-field. From an application standpoint, the coupling of spontaneous emission directly to the free space without passing through a cavity mode and mirrors offers faster response. This concept is particularly useful, when the operation speed is favored over overall efficiency and quantum yield.

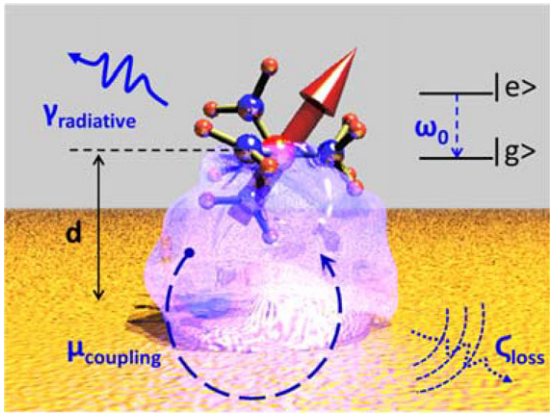

Figure 1 Schematics of an open resonator – fluorescent molecule with a dipolar transition is coupled to a surface. Coupling mechanisms, coefficients and geometrical parameters are indicated on the figure.

The letter is organized as follows–first, the general theoretical framework, applicable for any type of open resonator, will be developed. Next, it will be applied on the case of spontaneous emission next to a planar surface, where surface plasmon resonance condition is approached. Outlook and conclusions will be given at the end.

2 Theoretical framework

Modal structure of a cavity could be rather involved and encapsulate both far-field radiation and losses. While modal approaches for plasmonic cavities [34] and hybrid systems [22] could be employed, it is convenient to make a detailed separation of contributing mechanisms at the very beginning. The Hamiltonian of an open resonator + emitter contains several contributions. Apart from energies of isolated systems of an emitter ($\hat{\mathrm{H}}_E$), free electromagnetic field ($\hat{\mathrm{H}}_F$), cavity mode ($\hat{\mathrm{H}}_C$), and dissipation bath ($\hat{\mathrm{H}}_D$), there are several coupling mechanisms. The first one couples the emitter to the cavity mode ($\hat{\mathrm{H}}_{E-C}$), the cavity mode undergoes decay described by coupling to a heat bath $\hat{\mathrm{H}}_{C-D}$, and the emitter is directly coupled to the radiation field - $\hat{\mathrm{H}}_{E-F}$. The expressions for the above quantities are given by:

$$\hat{\mathrm{H}}_E = \hbar\frac{\omega_0}{2}\hat{\sigma}_0; \quad \hat{\mathrm{H}}_F = \sum_k \hbar\omega_k \hat{f}_k^\dagger \hat{f}_k; \quad \hat{\mathrm{H}}_C = \hbar\omega_c \hat{c}^\dagger \hat{c};$$

$$\hat{\mathrm{H}}_D = \sum_k \hbar\omega_k \hat{d}_k^\dagger \hat{d}_k; \quad \hat{\mathrm{H}}_{E-C} = \hbar\mu\left(\hat{c}^\dagger\hat{\sigma}_- + \hat{\sigma}_+\hat{c}\right);$$

$$\hat{\mathrm{H}}_{C-D} = i\hbar \sum_k \zeta_k \left[\hat{c}^\dagger \hat{d}_k - \hat{d}_k^\dagger \hat{c} \right];$$

$$\hat{\mathrm{H}}_{E-F} = i\hbar \sum_k \gamma_k \left[\hat{f}_k^\dagger \hat{\sigma}_- - \hat{\sigma}_+ \hat{f}_k \right];$$

$$\hat{\mathrm{H}}_{tot} = \hat{\mathrm{H}}_E + \hat{\mathrm{H}}_F + \hat{\mathrm{H}}_C + \hat{\mathrm{H}}_D + \hat{\mathrm{H}}_{E-C} + \hat{\mathrm{H}}_{C-D} + \hat{\mathrm{H}}_{E-F} \quad (1)$$

where ω_0 is the frequency of the emitter's resonant transition, $\hbar\omega_i$ corresponds to the energy of 'i's involved quanta with related creation/annihilation operators (defined with $\wedge$), $\hat{\sigma}_+$ and $\hat{\sigma}_-$ are Pauli rising and lowering operators, $\hat{\sigma}_0 = diag\{1, -1\}$, and coupling constants are μ, ζ_k, and γ_k. Set of Eqs.1 could be considered as an extended Jaynes–Cummings model [2] with several coupling mechanisms. $\hat{\mathrm{H}}_D$ encapsulates all dissipative processes of the cavity mode, related to non-far-field-radiative mechanisms, such as Joule losses, inter-mode coupling and others. $\hat{\mathrm{H}}_F$ defines far-field modes. This separation is made in order to obtain the dynamics of the emitted optical power. The set of Eqs. 1 assumes the existence of one discrete cavity mode ($\hat{\mathrm{H}}_C$), while the rest electromagnetic far-field radiation is treated as an infinite set ($\hat{\mathrm{H}}_F$). The extension of the model to several cavity modes is straightforward and could be done on the expense of algebraic complexity.

The strength of coupling coefficients in Eq. (1) have the curtail influence on the true eigen states of the total Hamiltonian. Those collective quantum operators could be decomposed into a weighted linear superposition of creation/annihilation operators of the initial system. Representing the model in the basis of uncoupled states enables addressing transient processes of different kinds. The only assumption is the thermal equilibrium of the bath, but not of a system, coupled to it. Characteristic times for achieving the bath-system equilibrium could vary significantly (usually from femto to pico- second scales, depending on the coupling nature, e.g. [35]), and the transient behavior could be captured by the model. In fact, values of coupling constants μ, ζ_k and γ_k could be extracted from experimental data and calculations, involving complex solutions of coupled Maxwell-Schrödinger dynamics. However, those parameters could be estimated by applying general arguments, as will be demonstrated in Section 3.

The model of Eqs. 1 could be further extended and additional coupling mechanisms could be included. For example, emitter-decay Hamiltonian $\hat{\mathrm{H}}_{E-D}$ could account for all nonradiative dissipative processes, e.g. nonradiative quenching, excited state depopulation due to scattering on phonons, and other probable solid state processes [35]. Impact of phonons on spontaneous emission dynamics in a cavity was recently studied [4]. Furthermore, direct decay of cavity mode into far field ($\hat{\mathrm{H}}_{C-F}$) could describe scattering from imperfections in the case of flat geometries or structured surfaces, and multipolar radiation from localized objects. Those effects, however, could be neglected if deep nano-scale objects are considered (e.g. [10, 36]).

The coupling between discrete-spectrum operators of the emitter-cavity system with the continuum of degrees of freedom, corresponding to the free electromagnetic field, could be described by introducing quantum stochastic analysis [37]. For example, atom-field coupling could be written in the form of stochastic Hamiltonian as:

$$\hat{\mathrm{H}}_{E-F} = i\hbar\sqrt{\gamma}\left(\hat{f}^\dagger(t)\,\hat{\sigma}_-(t) - \hat{\sigma}_+\,\hat{f}(t)\right), \quad (2)$$

where $\hat{f}(t)$ and $\hat{f}^\dagger(t)$ are *stochastic* field operators of annihilation and creation, obeying canonical commutation relations - $[\hat{f}(t), \hat{f}^\dagger(t)] \sim \delta(t - t')$. The corresponding quantum Wiener process is defined as $\hat{F}(t, t_0) = \int_{t_0}^{t} \hat{f}(t')dt'$ with the following conditions to hold-$d\hat{F}(t)d\hat{F}(t) = d\hat{F}^\dagger(t)d\hat{F}^\dagger(t) = 0$, $d\hat{F}(t)d\hat{F}^\dagger(t) = (\bar{N}_{th} + 1)dt$ and $d\hat{F}^\dagger(t)d\hat{F}(t) = \bar{N}_{th}dt$, where $\bar{N}_{th}$ is the thermal photon occupation number, approximated to be zero hereafter. First Markov approximation of the frequency-independent coupling constant was employed for deriving Eq. (2) [37]. The formalism of quantum stochastic differential equations (QSDE) enables obtaining expressions for system's propagator and deriving general expressions for operators' time evolution, e.g. [4, 37]. In order to underline the relative transparency of the stochastic Hamiltonian approach, the time evolution of an arbitrary operator $\hat{\Theta}$, governed by Eq. (2) is given by:

$$\begin{aligned} d\hat{\Theta} \approx{}& \sqrt{\gamma}\left[\hat{\Theta}(t), \left(d\hat{F}^\dagger\hat{\sigma}_- - \hat{\sigma}_+ d\hat{F}\right)\right] + \\ & \gamma\left(\hat{\sigma}_+\hat{\Theta}\sigma_-\left(\bar{N}_{th}+1\right) + \hat{\sigma}_-\hat{\Theta}\hat{\sigma}_+\bar{N}_{th}\right)dt - \\ & -\frac{1}{4}\gamma\hat{\sigma}_0\hat{\Theta}dt - \frac{1}{4}\gamma\hat{\Theta}\hat{\sigma}_0 dt - \gamma\left(\bar{N}_{th} + \frac{1}{2}\right)\hat{\Theta}dt, \end{aligned} \quad (3)$$

where γ is the collective decay rate to all available radiation modes. Substitution of $\hat{\Theta} = \hat{\sigma}_0$ leads to a simple differential equation for the population ($P_e = \frac{\langle\hat{\sigma}_0\rangle+1}{2}$) $\frac{dP_e}{dt} = -\gamma P_e$, showing exponential spontaneous decay in the case of vanishing thermal noise. The same result could be obtained with Weisskopf-Wigner approach, e.g. [2]. It should be noted, that the above example (Eq. (3)) corresponds to the emitter-free field coupling only. The entire systems' Hamiltonian (Eq. (1)) will lead (after some algebra) to the following set of coupled equations for operators' expectation values, denoted by <>:

$$\frac{d}{dt}\begin{pmatrix}\langle\hat{c}^{\dagger}\hat{c}\rangle\\ \langle\hat{\sigma}_0\rangle\\ \langle\hat{A}_1\rangle\\ \langle\hat{A}_2\rangle\end{pmatrix}=\begin{pmatrix}-\zeta & 0 & \mu & 0\\ 0 & -\gamma\left(2\bar{N}_{th}+1\right) & -2\mu & 0\\ 0 & \mu & -\left(\gamma\left(\bar{N}_{th}+\frac{1}{2}\right)+\frac{\zeta}{2}\right) & 2\mu\\ -\gamma & 0 & -\mu & -\left(2\gamma\left(\bar{N}_{th}+\frac{1}{2}\right)+\zeta\right)\end{pmatrix}\begin{pmatrix}\langle\hat{c}^{\dagger}\hat{c}\rangle\\ \langle\hat{\sigma}_0\rangle\\ \langle\hat{A}_1\rangle\\ \langle\hat{A}_2\rangle\end{pmatrix}+\begin{pmatrix}0\\ -\gamma\\ \mu\\ 0\end{pmatrix}, \tag{4}$$

where the following auxiliary operators were defined - $\hat{A}_1 = i(\hat{\sigma}_+\hat{c} - \hat{c}^{\dagger}\hat{\sigma}_-)$ and $\hat{A}_2 = \hat{c}^{\dagger}\hat{\sigma}_0\hat{c}$. Resonant condition $\omega_0 = \omega_c$ was also assumed and multiple photon excitations were neglected [2]. The set of Eq. (4) is solved by applying Laplace transform technique and the solution for system operators' expectation values is given by:

$$\begin{aligned}\left\langle\hat{c}^{\dagger}(t)\,\hat{c}(t)\right\rangle &= -\frac{8\mu^2}{C_1^2}e^{-\frac{\gamma+\zeta}{2}t}\left(1-\cosh\left(\frac{C_1}{2}t\right)\right),\\ \langle\hat{\sigma}_0(t)\rangle &= -\frac{16\mu^2}{C_1^2}e^{-\frac{\gamma+\zeta}{2}t}-\frac{2}{C_1^2}e^{-\frac{\gamma+\zeta}{2}t}\\ &\left(C_2\cosh\left(\frac{C_1}{2}t\right)+C_1(\gamma-\zeta)\sinh\left(\frac{C_1}{2}t\right)\right)-1,\end{aligned} \tag{5}$$

where $C_1 = \sqrt{-16\mu^2 - 2\gamma\zeta + \gamma^2 + \zeta^2}$ and $C_2 = 8\mu^2 + 2\gamma\zeta - \gamma^2 - \zeta^2$. The system's initial conditions are – emitter in its excited state and field occupation number is 0. The time-dependent cumulative energy fraction (expectation value), emitted to the far field, is given by $\frac{dI_F}{dt} = \gamma\frac{\langle\sigma_0+1\rangle}{2} = \gamma P_e$. The knowledge of the population's evolution (P_e) dynamics enables investigating impact of the strong coupling between the cavity and emitter (μ), cavity and radiative decays (ζ and γ) on spontaneously emitted photons, to be detected in the far-field.

First, the interplay between μ, ζ and γwill be studied without relating their values to any specific physical system. All the quantities in this section are dimensionless in order to represent a larger span of possible phenomena; numerical example will be given in the next section, where emission dynamics next to planar interfaces will be considered in details. Strong coupling regime is obtained when the value of emitter-cavity coupling μ become comparable with the collective decay rate $\gamma + \zeta$, as it could be seen from Eq. (5). In this case parameter C_1 becomes complex-valued. Enhancement of radiative rate, as the function of μ and ζ, appears as a log-scale plot on Fig. 2(a) (a time, when a half of total intensity is emitted to the far field (cumulative energy fraction)). γin all subsequent investigations was kept to be 1, in order to underline the impact of the strong/weak coupling and dissipation. First, the impact of μ and $\zeta$is asymmetric, as could be also seen from the main result-Eq. (5). The maximal enhancement is obtained in the strong coupling regime with high dissipative losses. Here, the population dynamics is solely defined by this complex nonradiative process, which enforces faster radiation. It should be noted, however, that this type of enhancement comes at the price of losses. Nevertheless, this approach could be of a use for applications where an operation speed is more important than a signal's intensity. Similar considerations are applied for designs of fast lasers, where Q-factors are decreased on purpose, introducing additional losses per round trip [38]. The normalized far-field radiated cumulative energy fraction, as the function of time, is shown in Fig. 2(c). The fastest population decay is obtained for the cases of strong coupling and moderate coupling with strong dissipation losses. Quantum yield, calculated for each intensity curve on Fig. 2(c) appears in the inset. The general observed trend is the reduction of the quantum yield with increase of the cavity coupling. This effect is attributed to the fact that the polariton mode of the resonator has higher occupation number in this case and stays for longer in the lossy medium, reducing the overall energy, emitted to the far field. The continuous increase of the material losses has, however, non-monotonous impact on the quantum yield (green and blue lines on Fig. 2 (c)). The difference between the pairs $\mu = 1$, $\zeta = 1$ and $\mu = 1$, $\zeta = 10$ is the regime of the interaction – strong/moderate coupling in the first case and weak coupling in the later one. Quantum yield in the strong/moderate case is lower, since the energy exchange between the emitter and polariton damps the energy more efficiently, than the simple exponential decay ($\mu = 1$, $\zeta = 10$ case).

The performance of the open type of resonator (the emitter is directly coupled to the far-field radiation) will be compared next to the classical scenario, where the far-field emission is obtained via the leakage of the cavity photon. In this case γ was set to zero and the cumulative energy fraction was calculated as $\frac{dI_F}{dt} = \gamma_{leak}\langle\hat{c}^{\dagger}(t)\hat{c}(t)\rangle$ with $\gamma_{leak} = 1$ for the direct comparison with the previous results ($\zeta_{total} = \zeta + \gamma_{leak}$). Fig. 2(b) shows the log-scale plot of the radiation rate enhancement in a closed cavity with a leakage. While

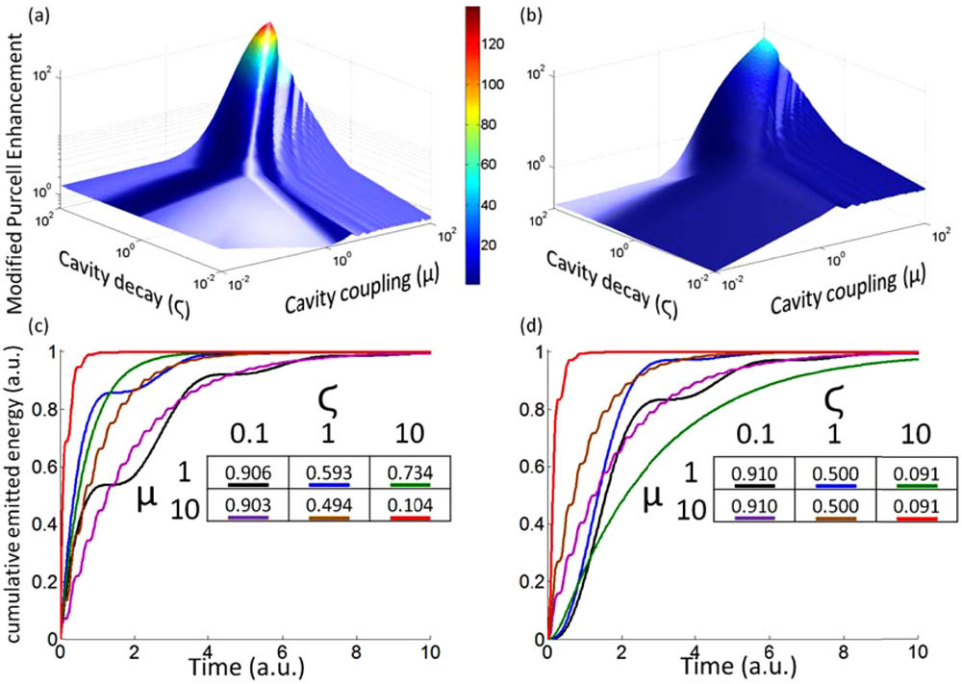

Figure 2 Radiative time dynamics in general resonators and cavities. Time, when a half of the cumulative energy is emitted to the far-field, as the function of cavity decay ζ and cavity coupling μ – (a) open resonator, (b) cavity. Time is in the log scale. (c and d) – cumulative power, as the function of time – various lines correspond to different system's parameters in the caption. Inset – quantum yield. (c) Open resonator, (d) cavity.

the general peaked structure remained similar to this of the open resonator scenario, the overall values of the enhancement are almost twice smaller. The result could be intuitively understood from the fact, that the photon should undertake several round trips in the cavity (given by its Q-factor) before leaving it and, as the result the overall radiation rate enhancement goes down. At the same time, in open resonators photons are directly emitted to the far field. The direct comparison of time-dependent curves (Fig. 2(c and d)) verifies this behavior. Quantum yield in the case of a closed cavity (inset in Fig. 2(d)) does not depend on the coupling strength, as there are no other channels to decay, rather than in to the cavity mode (other nonradiative mechanisms, considered in Ref. [4], are neglected). Hence, the quantum yield, being solely defined by the competition between the cavity leakage and its inherent losses, drops with the increase of ζ.

The general framework, developed here, enables addressing dynamics in realistic physical systems by estimating values of coupling and dissipation coefficients. In particular, spontaneous emission and nonradiative quenching in spasers (e.g. [23]) and nanolasers (e.g. [27]) could be analyzed fully quantum mechanically. Additional class of problems, required such an analysis, is related to planar surfaces and will be analyzed next.

3 Coupled dynamics in planar resonators

Planar geometries are of special interest due to variety of new emerging applications, e.g. [39, 40], motivating further investigations of light-matter interaction dynamics in their vicinity. Being a subject for numerous studies (e.g. [41]), modification of spontaneous emission next to a plane surface was analyzed by means of competitive decay channels for the most. This approach, however, relies on the hard assumption of Markovian exponential dynamics, predefined by the fastest decay mechanism. The immediate implication of this approach is that a fast nonradiative quenching will speed up the radiation to the far-field on the expense of the overall quantum yield. While the unified approach, developed above, gives exactly the same conclusion for the weak coupling regime with the surface, it also enables revealing non-exponential channels, related to the strong coupling and complex decay dynamics. Note that a

sufficient near-field feedback could result in non-exponential law of decay in various systems, e.g. [36].

Decay rates in the weak coupling regime are proportional to LDOS, given by an imaginary part of electromagnetic Green function [5]. Radiative decay and nonradiative quenching channels could be separated by integrating the near- and far-field contribution of a classical dipole by enclosing it by a pair of small and large integration surfaces. In the case of a planar geometry, radiative rate has relatively simple and intuitive expression, derived with the help of Lorentz reciprocity theorem [42]. The expression for the radiative rate enhancement (to the upper half-space) of a dipole, oriented perpendicular to the surface is given by [42]:

$$\Gamma^{\perp} = \frac{3}{4}\int_0^{\frac{\pi}{2}} \left|1 + r^p(\theta)\, e^{2ik_0 d\cos\theta}\right|^2 \sin^3\theta\, d\theta, \tag{6}$$

where r^p is the Fresnel reflection coefficient for TM-polarized waves (magnetic field parallel to the surface), k_0 is the wavevector in the material above the pane (assumed to be vacuum here), d is the distance between the dipole and the surface, and θ is the angle with respect to the surface's normal. Similar expression for $\Gamma^{\parallel}$ can be written for a dipole, parallel to the surface [42]. It can be seen by setting an upper limit on the integrand of Eq. (6) that the radiative rate enhancement (to the upper half space, including the dipole) cannot exceed the factor of 2. The maximal enhancement could be obtained with a perfectly reflecting mirror, while the fundamental limitation on both $\Gamma^{\perp}$ and $\Gamma^{\parallel}$ comes from the conservation law of a wave's energy, reflected from a surface. It is worth underlining several important points. First, Fresnel reflection coefficients could be defined for any flat geometry having translational symmetry along the surface. Hence, the above limitation is not applicable for irregularly patterned surfaces, such as gradient metasurfaces, for example [43, 44]. Second, the *overall* emission rate could be enhanced with planar geometries, e.g. layered hyperbolic metamaterials [45], but the majority of the radiation will be trapped in the substrate, while the field, emitted to the upper half-space will not gain any significant enhancement. Finally, the rate enhancement factor has a physical meaning only in the weak coupling regime of interaction, when the Fermi Golden Rule can be applied. The goal of the forthcoming analysis is to bypass the limitations on $\Gamma^{\perp}$ and $\Gamma^{\parallel}$, by considering strong coupling regime of interaction and applying the formalism, developed for open resonators.

The regime of strong coupling between emitters and plasmonic structures could be reached with relatively low-Q resonators by getting an advantage on small modal volumes [13–18]. In the case of planar geometry the resonant condition is obtained when permitivities of the lower (ε_m) and the upper (ε_d) half-space have opposite signs of real parts, namely $\mathrm{Re}(\varepsilon_d) = -\mathrm{Re}(\varepsilon_m)$. In this case, surface wave has vanishing phase velocity and the resonance is created due to the light stopping effect, e.g. [29]. Emission dynamics for both cases of the dipolar orientation, namely perpendicular and parallel to the surface, will be considered next. The set of parameters, required for the full quantum analysis was obtained in the following way $-\frac{\gamma}{\gamma_0}$ was taken to be either $\Gamma^{\perp}$ or $\Gamma^{\parallel}$, where γ_0 was taken to be a typical spontaneous emission rate corresponding to 1 ns lifetime. The overall decay rate of the dipole with radiative contribution subtracted provides the cavity coupling μ (nonradiative quenching). This approach could be directly related to spectral density concept, e.g. [46, 47]. It is worth noting, that the developed method gives the link to separate the spectral density of the resonator modes from all the radiative ones. The damping of the cavity mode was approximated with widely accepted value of $Q \sim -\frac{\mathrm{Re}(\varepsilon_m)}{\mathrm{Im}(\varepsilon_m)}$, without going into details of dispersion and geometry [10]. Fig. 3 summarizes the spontaneous emission rate enhancement as the function of $\mathrm{Im}(\varepsilon_m)$ and the distance d between the emitter and the surface. The emission wavelength is taken to be 500nm, while the material is not specified on purpose, in order to underline contributions of its various parameters. Fig. 3 (a and b) represent the time, when a half of total intensity is emitted to the far-field, normalized to either $\Gamma^{\parallel}\gamma_0$ for horizontally-oriented dipole (panel a) or $\Gamma^{\perp}\gamma_0$ for the vertical (panel b). The maximal enhancement (as defined above) reaches the values of 45000 for vertical dipole and almost twice smaller for horizontal. Remarkably, the maximal enhancement, increasing monotonically with reducing d, has nontrivial dependence on material losses. The enhancement has the peak around $\mathrm{Im}(\varepsilon_m) = 0.01$, while simple approach for exponential nonradiative quenching will suggest the monotonic increase with losses. Fig. 3 (c and d) show the population decay (logarithmic scale) as the function of time. Main graphs at those panels correspond to the weak coupling regime, hence the decay law is exponential (straight lines on the log-plots). The strong coupling dynamics appears on the insets and shows common damped oscillatory behavior. In the weak coupling regime, the fastest decay rate of the vertical dipole (among the set of 3 considered parameters) is obtained for the shortest d. For the horizontal dipole, however, the shortest d results in the slowest decay. This result is the combination of the radiation efficiency, which strongly

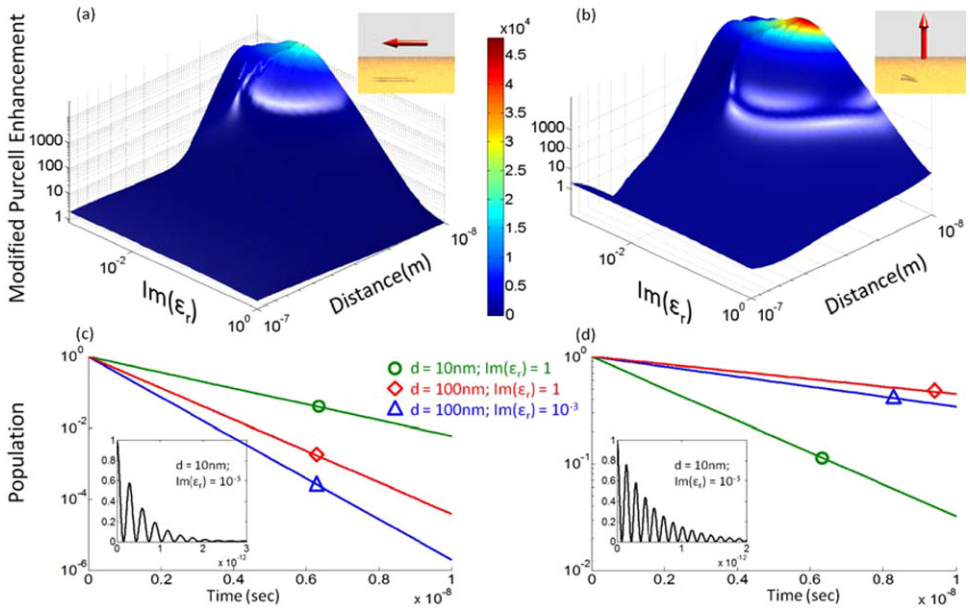

Figure 3 Radiative time dynamics of an emitter (dipole) next to a surface. Time, when a half of the cumulative energy is emitted to the far-field, as the function of material losses $\mathrm{Im}(\varepsilon_m)$ (substrate material with $\mathrm{Re}(\varepsilon_m) = -1$) and the distance from the emitter to the surface d. (a) horizontal dipole; (b) vertical dipole. Times in the log scale are normalized to either $\Gamma^{\parallel}\gamma_0$ for horizontally-oriented dipole or $\Gamma^{\perp}\gamma_0$ for the vertical. (c and d) – logarithm of the population as the function of time for several system's parameters (weak coupling regime), indicated in the upper inset. Insets – strong coupling regime of interaction – population (normal scale) as the function of time.

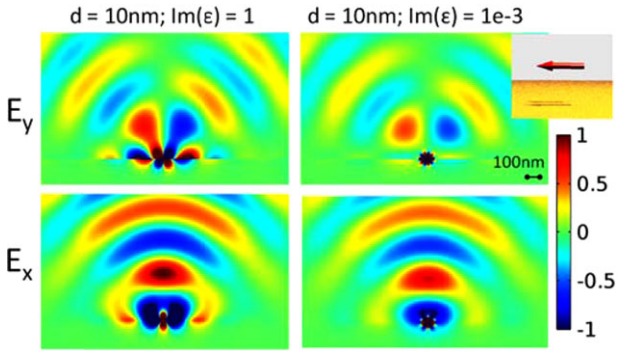

Figure 4 Field patterns of the horizontally polarized dipole (field snapshot). Field components and material parameters are organized in the table. Y is the direction, perpendicular to the surface, while X-axis is parallel to it. All the 4 panels were normalized to the same value, shared with Fig. 5.

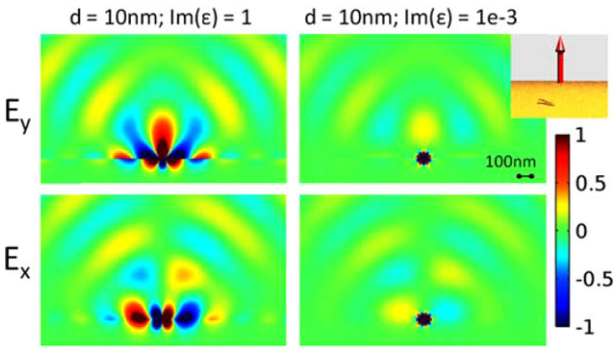

Figure 5 Field patterns of the vertically polarized dipole (field snapshot). Field components and material parameters are organized in the table. Y is the direction, perpendicular to the surface, while X-axis is parallel to it. All the 4 panels were normalized to the same (arbitrary) value, shared with Fig. 4.

depends on the orientation, and the efficiency of the excitation of the resonator mode. In order to emphasize this effect, finite element frequency domain simulation (Comsol software) for two-dimensional dipoles was performed. Fig. 4 shows major field components (field snapshot at an arbitrarily chosen moment of time) for the horizontal dipole, situated next to surfaces with high and low losses. Fig. 5 shows the same for the vertical dipole. In both cases, small losses enable supporting the excitation of highly localized resonator modes – the key for achieving strong coupling. It is worth noting, that the classical simulation of this type enables calculation of μ, γ and ζ coefficients, but is not capable to cope with complex quantum dynamics. In the high loss case the modes are much less confined and the weak coupling regime regulates the dynamics. The amplitudes of the fields (especially imaginary part of Green function – LDOS) should not be confused with the rate of decay, as

it was already underlined several times. The dynamics could be controlled by nonradiative transitions and strong coupling. In all the above considerations, emitters were not brought too close to the surface, as at distances smaller than 10 nm additional quenching mechanisms could begin playing key roles, e.g. [48, 49]. It should be noted, however, that quenching mechanisms strongly depend on system's realization. Recent reports and analysis show strong Purcell enhancements in small gaps without dramatic nonradiative quenching [50–53]. Note, that the angular dependence of the emission, usually addressed with the spectral density of states concept (e.g. [54]), could be evaluated with selective favoring of one from the emission channels in the Hamiltonian $\hat{H}_{E-F}$ Eq. (1).

4 Outlook and conclusion

Full quantum mechanical treatment of spontaneous decay dynamics of emitters, situated in a vicinity of open resonators was developed. Stochastic Hamiltonian approach enables treating decay channels in relatively straightforward form and, at the same time, preserves canonical commutation relations between creation and annihilation operators of lossy plasmonic excitations. Furthermore, quantum description opens a room for discovering new unrevealed regimes, like the one described here. The time evolution law of interaction between emitters and open resonators was formulated with the help of three major coefficients, which could be calculated either numerically of estimated from the first principles. The developed theory was subsequently applied to the process of spontaneous emission near planar surfaces. Those inherently open structures were shown to provide substantial acceleration of spontaneous emission, which goes beyond the fundamental limits, set by the weak coupling regime of interaction. It was shown, that nonradiative quenching and strong coupling could significantly affect the emission times on the expense of reduced quantum yield.

From the fundamental standpoint, the formalism enables straightforward analysis of open resonators, being basic building blocks for spasers and nano-lasers. In fact, though closed configuration may be better for good spasers [10, 30, 32], technological aspects may still favor open geometries. Gap structures (e.g. [9, 52]) could facilitate aching spasing conditions. From the application side, measurements of lifetimes, being much more robust and reliable technique than intensity detection, are routinely used for bio-imaging purposes. For example, plasmonic particles functionalized with fluorophores enable achieving high quality imaging, e.g. [55]. Full quantum description of such hybrid fluorescent labels can further improve imaging limits.

Acknowledgments. The author acknowledges support from TAU Rector Grant, German-Israeli Foundation (GIF, grant number 2399). The work was supported in part by the Russian Science Foundation (No. 14-12-01227 (numerical calculations of electromagnetic fields)), the Russian Fund for Basic Research (project #15-02-01344), Government of the Russian Federation (No. 074-U01).

References

[1] E. M. Purcell, Phys. Rev. **69**(11–12), 674–674, (1946).
[2] M. O. Scully and M. S. Zubairy, Quantum Optics. Cambridge University Press, (1997).
[3] R. Ameling and H. Giessen, Laser Photon. Rev. **7**(2), 141–169 (2013).
[4] P. Ginzburg, A. V. Krasavin, D. Richards, and A. V. Zayats, Phys. Rev. A **90**(4), 043836 (2014).
[5] W. Vogel and D.-G. Welsch, Quantum Optics. Wiley-VCH; 3rd, Revised and Extended Edition edition, (2006).
[6] R. Carminati, A. Cazé, D. Cao, F. Peragut, V. Krachmalnicoff, R. Pierrat, and Y. De Wilde, Surf. Sci. Rep. **70**(1), 1–41 (2015).
[7] K. J. Vahala, Nature **424**(6950), 839–846 (2003).
[8] D. K. Gramotnev and S. I. Bozhevolnyi, Nat. Photonics **4**(2), 83–91 (2010).
[9] P. Ginzburg, D. Arbel, and M. Orenstein, Opt. Lett. **31**(22), 3288–3290, 2006.
[10] M. I. Stockman, Opt. Express **19**(22), 22029–22106 (2011).
[11] E. Feigenbaum and M. Orenstein, Phys. Rev. Lett. **101**(16), 163902 (2008).
[12] L. Novotny and N. van Hulst, Nat. Photonics **5**(2), 83–90 (2011).
[13] N. Berkovitch, P. Ginzburg, and M. Orenstein, Journal of Physics: Condensed Matter **24**(7), 073202 (2012).
[14] I. Pockrand, J. Chem. Phys. **77**(12), 6289 (1982).
[15] T. K. Hakala, J. J. Toppari, A. Kuzyk, M. Pettersson, H. Tikkanen, H. Kunttu, and P. Törmä, Phys. Rev. Lett. **103**(5), 053602 (2009).
[16] A. Berrier, R. Cools, C. Arnold, P. Offermans, M. Crego-Calama, S. H. Brongersma, and J. Gómez-Rivas, ACS Nano **5**(8), 6226–6232 (2011).
[17] S. Aberra Guebrou, C. Symonds, E. Homeyer, J. C. Plenet, Y. N. Gartstein, V. M. Agranovich, and J. Bellessa, Phys. Rev. Lett. **108**(6), 066401 (2012).
[18] P. Vasa, W. Wang, R. Pomraenke, M. Lammers, M. Maiuri, C. Manzoni, G. Cerullo, and C. Lienau, Nat. Photonics **7**(2), 128–132 (2013).
[19] A. Shalabney, J. George, J. Hutchison, G. Pupillo, C. Genet, and T. W. Ebbesen, Nat. Commun. **6**, 5981 (2015).

[20] A. Manjavacas, F. J. García de Abajo, and P. Nordlander, Nano Lett. **11**(6), 2318–2323 (2011).
[21] X.-W. Chen, V. Sandoghdar, and M. Agio, Phys. Rev. Lett. **110**(15), 153605 (2013).
[22] J. Yang, M. Perrin, and P. Lalanne, Phys. Rev. X **5**(2), 021008 (2015).
[23] D. Bergman and M. Stockman, Phys. Rev. Lett. **90**(2), 027402 (2003).
[24] M. A. Noginov, G. Zhu, A. M. Belgrave, R. Bakker, V. M. Shalaev, E. E. Narimanov, S. Stout, E. Herz, T. Suteewong, and U. Wiesner, Nature **460**(7259), 1110–1112 (2009).
[25] X. Meng, A. V Kildishev, K. Fujita, K. Tanaka, and V. M. Shalaev, Nano Lett. **13**(9), 4106–4112 (2013).
[26] M. T. Hill, Y.-S. Oei, B. Smalbrugge, Y. Zhu, T. de Vries, P. J. van Veldhoven, F. W. M. van Otten, T. J. Eijkemans, J. P. Turkiewicz, H. de Waardt, E. J. Geluk, S.-H. Kwon, Y.-H. Lee, R. Nötzel, and M. K. Smit, Nat. Photonics **1**(10), 589–594 (2007).
[27] R. F. Oulton, V. J. Sorger, T. Zentgraf, R.-M. Ma, C. Gladden, L. Dai, G. Bartal, and X. Zhang, Nature **461**(7264), 629–632 (2009).
[28] M. Khajavikhan, A. Simic, M. Katz, J. H. Lee, B. Slutsky, A. Mizrahi, V. Lomakin, and Y. Fainman, Nature **482**(7384), 204–207 (2012).
[29] T. Pickering, J. M. Hamm, A. F. Page, S. Wuestner, and O. Hess, Nat. Commun. **5**, 4972 (2014).
[30] J. B. Khurgin and G. Sun, Nat. Photonics **8**(6), 468–473 (2014).
[31] E. I. Galanzha, R. Weingold, D. A. Nedosekin, M. Sarimollaoglu, A. S. Kuchyanov, R. G. Parkhomenko, A. I. Plekhanov, M. I. Stockman, and V. P. Zharov, "Spaser as Novel Versatile Biomedical Tool," *http://arxiv.org/abs/1501.00342*, (2015).
[32] M. I. Stockman, J. Opt. **12**(2), 024004 (2010).
[33] T. P. H. Sidiropoulos, R. Röder, S. Geburt, O. Hess, S. A. Maier, C. Ronning, and R. F. Oulton, Nat. Phys. **10**(11), 870–876 (2014).
[34] C. Sauvan, J. P. Hugonin, I. S. Maksymov, and P. Lalanne, Phys. Rev. Lett. **110**(23), 237401 (2013).
[35] D. W. Snoke, Solid State Physics: Essential Concepts, 1 edition. Addison-Wesley, (2008).
[36] P. Ginzburg and A. V. Zayats, Optics Express **20**(6), 6720 (2012).
[37] C. Gardiner and P. Zoller, Quantum Noise - A Handbook of Markovian and Non-Markovian Quantum Stochastic Methods with Applications to Quantum Optics, 3rd ed. Springer-Verlag, Berlin Heidelberg, (2004).
[38] M. L. M. Larry A. Coldren, Scott W. Corzine, Diode Lasers and Photonic Integrated Circuits, 2 edition. Wiley, (2012).
[39] N. Yu and F. Capasso, Nat. Mater. **13**(2), 139–150 (2014).
[40] A. V Kildishev, A. Boltasseva, and V. M. Shalaev, Science **339**(6125), 1232009 (2013).
[41] G. W. Ford and W. H. Weber, Surf. Sci. **109**(2), 451–481 (1981).
[42] E. Le Ru and P. Etchegoin, Principles of Surface-Enhanced Raman Spectroscopy: and related plasmonic effects, 1st ed. Elsevier Science, (2008).
[43] D. Lin, P. Fan, E. Hasman, and M. L. Brongersma, Science (80-.). **345**(6194), 298–302 (2014).
[44] S. Sun, Q. He, S. Xiao, Q. Xu, X. Li, and L. Zhou, Nat. Mater. **11**(5), 426–431 (2012).
[45] O. Kidwai, S. V Zhukovsky, and J. E. Sipe, Opt. Lett. **36**(13), 2530–2532 (2011).
[46] D. Dzsotjan, A. S. Sørensen, and M. Fleischhauer, Phys. Rev. B **82**(7), 075427 (2010).
[47] T. Hümmer, F. J. García-Vidal, L. Martín-Moreno, and D. Zueco, Phys. Rev. B **87**(11), 115419 (2013).
[48] W. L. Barnes, J. Mod. Opt. **45**(4), 661–699 (2009).
[49] E. Dulkeith, A. C. Morteani, T. Niedereichholz, T. A. Klar, J. Feldmann, S. A. Levi, F. C. J. M. van Veggel, D. N. Reinhoudt, M. Möller, and D. I. Gittins, Phys. Rev. Lett. **89**(20), 203002 (2002).
[50] K. J. Russell, T.-L. Liu, S. Cui, and E. L. Hu, Nat. Photonics **6**(7), 459–462 (2012).
[51] G. M. Akselrod, C. Argyropoulos, T. B. Hoang, C. Ciracì, C. Fang, J. Huang, D. R. Smith, and M. H. Mikkelsen, Nat. Photonics **8**(11), 835–840 (2014).
[52] R. Faggiani, J. Yang, and P. Lalanne, ACS Photonics **2**(12), acsphotonics.5b00424 (2015).
[53] J. Yang, R. Faggiani, and P. Lalanne, Nanoscale Horiz. **1**(1), 11–13 (2016).
[54] R. C. McPhedran, L. C. Botten, J. McOrist, A. A. Asatryan, C. M. de Sterke, and N. A. Nicorovici, Phys. Rev. E **69**(1), 016609 (2004).
[55] A. Saha, S. Basiruddin, R. Sarkar, N. Pradhan, and N. R. Jana, J. Phys. Chem. C **113**(43), 18492–18498 (2009).